A Reliability-Based Approach for the Design of Rockfall Protection Fences

Franck Bourrier, Stéphane Lambert, Julien Baroth

A Reliability-Based Approach for the Design of Rockfall Protection Fences

F. Bourrier, S. Lambert, J. Baroth

Abstract This paper proposes a method for improving the design of rockfall protection fences and accounting for the variability of loading cases. It is based on a probabilistic reliability analysis and can combine loading cases from rockfall propagation simulations with numerical simulations of the structure response to the block impact. The advantage of such a reliability-based approach is that statistically relevant results can be obtained concerning the fence's efficiency in stopping the block with a limited number of simulations. This method was employed in a study case, involving a low-energy tree-supported fence placed on a forested slope. The trajectory simulations were conducted using Rockyfor3D and the fence was modelled using a three-dimensional discrete element method model. For demonstration purposes, two parameters were considered: block velocity and the block's angle of incidence before impact. The probability of the fence stopping the block was evaluated accounting for the variability of these two parameters separately and together, either considering these variables as non-correlated, or as correlated. The value of this approach is demonstrated in terms of computation cost. In addition, the results revealed the importance of accounting for both these parameters in designing the structure as well as in estimating the residual hazard downslope from the protective structure.

F. Bourrier (✉)
Irstea, UR EMGR, 38402 St-Martin-d'Hères, France
e-mail: franck.bourrier@irstea.fr

S. Lambert
Irstea, UR ETGR, 38402 St-Martin-d'Hères, France
e-mail: stephane.lambert@irstea.fr

J. Baroth
Joseph Fourier University, Grenoble INP, UMR5521-3SRLab, DU, 38041 Grenoble cedex 9, France
e-mail: julien.baroth@ujf-grenoble.fr

Keywords Rockfall protection structures · Discrete element model · Reliability analysis

List of Symbols

Cv_i	Coefficient of variation of random variable X_i
$E_{c,\ \max}$	Estimated maximum block impact energy
F_{slip}	Cable clips sliding force
G	Performance function, associated with the limit state $G = 0$
$\tilde{G}$	Approximation of G
L_i	Lagrangian polynomial
m_{rock}	Block mass
P_f	Fence failure probability, equals Prob($G > 0$)
p_y	Probability density function of $\mathbf{Y}$
T	Gaussian standardization function
V_r	Block translational velocity at impact
$V_{r,\ \max}$	Estimated maximum block translational velocity at impact
$V_{z,\ \mathrm{out}}$	Norm of the block translational velocity after contact with the fence
$V_{z,\ \mathrm{in}}$	Norm of the block translational velocity before contact with the fence
$\mathbf{X}$	Vectorial Gaussian standard variable, related to $\mathbf{Y}$ such as $\mathbf{Y} = T(\mathbf{X})$
X_i	Components of Gaussian standard random variable $\mathbf{X}$
x_i	Realization (chosen value) of component X_i of vector $\mathbf{X}$
$\mathbf{Y}$	Vectorial random variable associated with the loading parameters
Y_i	Random variables
y_i	Uncertain parameters associated with the block properties and its trajectory
$\mathbf{Z}$	Vectorial random variable associated with the fence reponse

Greek Symbols

α_r Impact angle

λ_ϵ Reduction factor for the strain at rupture of double-twisted wires vs. single wire

λ_k Reduction factor for the stiffness of double-twisted wires vs. single wire

μ_i Mean value of the random variable Y_i

$\rho_{Y_iY_j}$ Correlation coefficient between the random variables Y_i and Y_j

σ_{Y_i} Standard deviation of the random variable Y_i

ω_r Norm of the block rotational velocity

1 Introduction

Protection against rockfall hazard often requires building passive protection structures, such as embankments or fences, forming obstacles on the block's route down the slope. The choice between these two countermeasure types is governed mainly by the block's kinetic energy and topographic constraints. Fences are widely used to protect roads, railways and buildings downhill of steep slopes, from rock blocks with energies up to 5,000 kJ and sometimes more.

Fences consist of an interception structure, a support structure and connecting components, most often made of metallic elements such as a net, posts and cables (EOTA 2008). For energies less than 100 kJ, support structures generally consist of fixed posts. For higher energies, cables anchored in the soil and connected to the top of the posts are necessary. Moreover, above a 500 kJ energy, friction brakes are used to reduce the force transmitted to these cables and their anchorage, with the aim of dissipating the energy while allowing large displacements of the fence.

Similar to embankments, fences must be designed so as to intercept the block trajectory and to withstand the impact, respectively referred to as functional and structural designs (Lambert and Bourrier 2013). Both these design aspects require data from rockfall propagation simulations. The trajectory simulation tools used for this purpose provide the design engineer with the statistical distributions of the passing height and velocity of a given block of a certain mass at any given point on the slope (Bourrier et al. 2009).

Classically, the functional design, which aims at defining the fence interception height, considers the block passing height distribution while the structural design mainly considers the block kinetic energy distribution. For both these parameters, a statistical estimator of the distribution is considered (95 % quantile, for example), so that only a very limited percentage of blocks are not caught by the structure or destroyed by it.

For the last two decades, rockfall protection fences have received substantial attention through experimental and numerical investigations (Hearn et al. 1996; Peila et al. 1998; Nicot et al. 2001; Gerber and Boell 2006; Volkwein et al. 2009; Gottardi and Govoni 2010; Bertrand et al. 2012; Tran et al. 2013; Thoeni et al. 2013). Reviews of these studies can be found in Gottardi and Govoni (2010) and Peila et al. (1998). The vast majority of the studies conducted to date concerns fences intended to intercept blocks with kinetic energies from 1 to more than 5,000 kJ given the very high demand for protection against catastrophic events. Rockfall fences designed for energies amounting to 200 kJ or less have been marginally studied even though they potentially concern a large number of sites (Cazzani et al. 2002; Buzzi et al. 2012; Spadari et al. 2013). The real-scale tests conducted within the technical agreement process covering fences in Europe (EOTA 2008) contribute to the research on the actual response of the flexible barriers and provides validation data for the numerical models developed (Bertrand et al. 2012; Gentilini et al. 2012).

Despite the recent advances in the impact response of fences, limitations concerning their design can be identified. In particular, the fence design rarely considers the block's trajectory before impact, that is the impact point location and the block kinematics when impacting the fence (trajectory inclination with respect to the fence, block rotational velocity, etc.). In addition, the variability associated with the different loading parameters is not accounted for. The numerous numerical tools that have been developed for modelling the impact response of fences could be used to analyse the response of the structure for loading cases representative of the distribution of the block trajectories before impact. However, from a practical point of view, such studies would require conducting a large number of simulations to obtain statistically relevant results, meaning expensive computation times.

This paper proposes an alternative methodology based on reliability analyses (Baroth et al. 2012) to overcome this key limitation to the use of numerical models for the design of rockfall protection fences. In the methodology proposed, probabilistic modelling of loading is deduced from the rockfall simulations. The probability of the fence stopping the block under probabilistic loading from the rockfall simulations is calculated from a small number of impact simulations using a specific probabilistic method (Baroth et al. 2007). The fence design methodology is applied to a case study focusing on two parameters identified as the most important the case study, namely the block impact velocity and the impact angle.

2 Study Case

The design methodology proposed was illustrated on a well-documented site for which the relevance of the block propagation simulations was assessed from field experiments. For illustration purposes, a particular type of rockfall protection fence with a previously developed numerical model of the fence was considered, although the methodology could be applied to different types of fences. This type of structure was developed for being installed on forested slopes where rockfall can be initiated by wood felling practices or above forest roads openings. The assement of this structure was based on real-scale impact tests conducted on an experimental site and using a numerical model of the structure, developed at the same time (Bourrier et al. 2010; Lambert et al. 2009).

2.1 Study Site

An extensively documented field rockfall experimental site was used. The study area covers an Alpine slope ranging from 1200 m to 1400 m above sea level with a 38° mean gradient in the 'Forêt Communale de Vaujany' in France (lat. 45°12′, long. 6°3′). The slope's surface mainly consists of rockfall deposits. For the analysis, the 3D rockfall simulation code Rockyfor3D was used. This software simulates the propagation of spherical falling blocks by successive phases of free flight and rebound on the slope surface on a digital terrain model from user-defined departure zones. Several studies simulating the rockfall experiments have been conducted (Dorren et al. 2006; Bourrier et al. 2009). In these studies, the topography of the site was modelled as a raster map, i.e., a gridded array of cells. Each cell represented a horizontal squared surface of the site and a mean elevation value was associated with this surface. The digital terrain model used was composed of 4 m^2 cells in order to keep the duration of the simulations reasonable while having a rather precise description of the whole site topography. This resolution is consistent with engineering practices (Crosta and Agliardi 2004; Agliardi et al. 2009). The parameters of the block rebound model had also been characterized for the different parts of the study site during field measurement campaigns. The values of these parameters and the digital terrain model used in the previous investigations on the study site (Dorren et al. 2006; Bourrier et al. 2009) were used in this study. The study case focuses on protecting the forest road located at mid-slope from 0.2 m^3 blocks (mass: 476 kg) (Fig. 1). The departure zone of the block is located 20 m above the forest road. In this context, the impact energy may remain less than 50 kJ. The initial falling height of the block was set at 0.5 m, assuming that the blocks were reactivated from small topographical outgrowths and the projected fence was located at an intermediate distance between the block release point and the forest road to be protected (Fig. 1).

The results from the rockfall simulations are intended to characterize the loading conditions of the fence. In the numerical model, the fence is assumed to be located at the limit between raster cells. Consequently, for each block release, the kinematics of the block was recorded at the time the block crosses the fence. All the quantities defining the block kinematics were measured along the block propagation plane. Along this plane, when reaching the

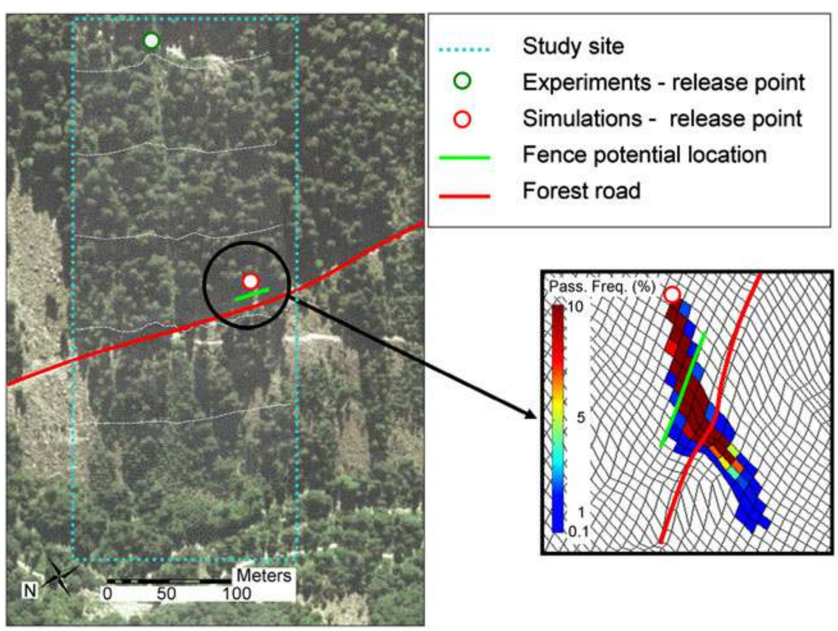

Fig. 1 Definition of the block release point and fence location in the simulations. On the 3D view of the simulations, the colours of the raster map cells depend on the frequency with which the blocks pass inside the cells (Pass. Freq.)

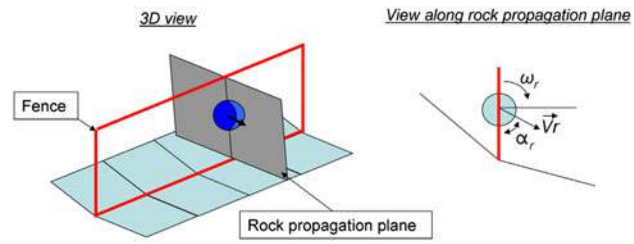

Fig. 2 Parameters describing the block trajectory when crossing the fence

fence, the block kinematics is fully characterized by the norm V_r of its translational velocity, the norm ω_r of its rotational velocity, and the impact angle α_r (Fig. 2). Figure 3 presents distributions of trajectographic characteristics resulting from simulations of the propagation of 100,000 rocks from the release point. These figures show significant variability in the kinematical parameters of the blocks when approaching the fence.

The design of the net based on a reliability approach should make it possible to define the fence failure probability (i.e., corresponding to a block not stopped) accounting for the variability of the kinematical parameters of the block V_r, α_r, and ω_r and of the impact point location characterized by the vertical and horizontal location of the block.

2.2 A Tree-Supported Structure for Low-Energy Impacts

The structure is a particular fence using existing trees in place of man-made posts to support the interception structure (Fig. 4). Its installation, therefore, does not require heavy machinery for soil moving or nailing, preserving the forest stand. Moreover, it is rapid and easy to install and remove, making these tree-supported structures an adequate solution for temporary protection purposes for instance during works on the slope. Using trees as supports instead of posts globally simplifies the installation. However, the design of the structure must account for the mechanical characteristics of the tree, which depend on the tree diameter and species (Dorren et al. 2006) and on the anchorage of the root system (Stokes et al. 2005). In addition, the selected trees must be at the same altitude to build a fence perpendicular to the average trajectory of the falling blocks, and at an appropriate distance from one another. Rockfall in this context may involve blocks with a mass ranging from 1 to less than 1,000 kg, with velocities less than 25 m/s, the maximum velocity of blocks on forested slopes reported in the literature (Dorren et al. 2006). The blocks' kinetic energy is, thus, less than 200 kJ, which is considered a low-energy value for rockfall protection structures. Spadari et al. (2013) also provide additional evidence that, in some environments, such low levels of

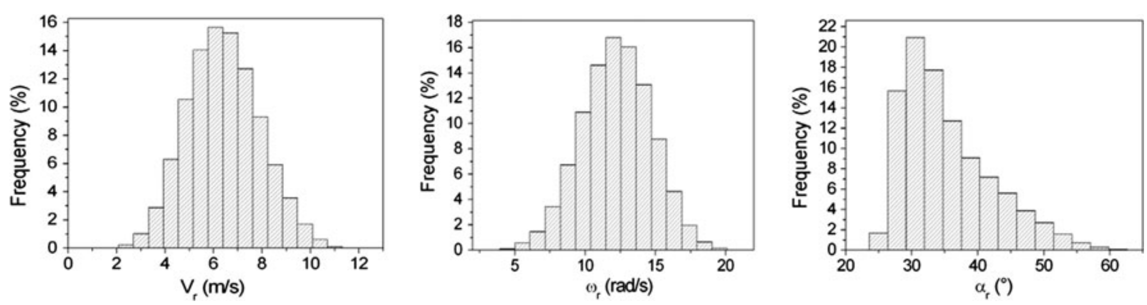

Fig. 3 Block kinematics when reaching the fence obtained from rockfall simulations: distributions of the translational velocity V_r, rotational velocity ω_r, and impact angle α_r

Fig. 4 Sketch of the experimental tree-supported fence (not to scale)

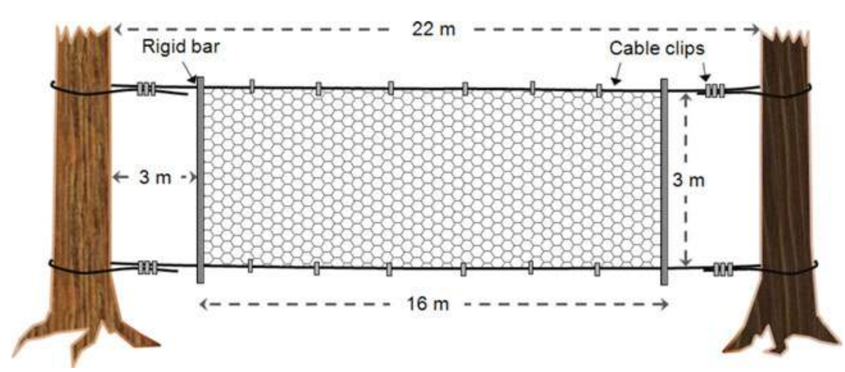

block kinetic energy are involved. The tested structure consists of two cables supporting a hexagonal wire mesh laterally lined by two bars. A double-twisted wire mesh as the interception structure was selected among various alternatives, because this product is widespread and easily available. It is widely used for active rockfall and surface erosion mitigation structures (Sasiharana et al. 2006). The mesh is made of a 2.7-mm-diameter wire forming hexagons 80 and 100 mm in height and width, respectively. The tensile strength of this wire netting is 51 kN/m. The interception structure is connected to both the upper and lower cables, 12 mm in diameter, using regularly spaced cable clips. The distance between the cables, or fence height, is 3 m. Each cable extremity forms a loop around a tree trunk, the cable dead end secured on the cable by three cable clips. The loops are loosely tightened to avoid any damage to the trunk. The distance between the upper and lower cables is maintained constant with the two rigid bars placed at each extremity of the wire mesh, parallel to the tree trunks. For the experiments, the distance between the trunks and the bars was 3 m but it can be reduced on real structures. The trees selected for supporting the structure were a spruce (*Picea abies*) 0.8 m in diameter and a maple (*Acer*) 0.6 m in diameter, 22 m apart. This distance is the average distance between trees in settled forest stands with similar trunk diameters. These parameters were considered in the numerical model presented hereafter and the experiments provided data for its calibration (Bourrier et al. 2010; Lambert et al. 2009).

2.3 Numerical Model of the Fence

The structure's response was simulated based on the discrete element method (DEM) (Cundall and Strack 1979) using the open-source software Yade-DEM (Smilauer et al. 2010). DEM models consider the structure as a set of particles interacting with each other. The interaction force between a pair of particles is computed at each time step from the interparticle distance resulting from the previous time step's calculations and considering the mechanical characteristics of the structure between the particles. Then the resultant of the forces acting on each particle is computed before deriving its displacement using Newton's second law.

The tree-supported fence was modelled accounting for the geometry of the fence, cables and bars, and the boundary conditions. The supporting trees were modelled as fixed points given that their displacement during the impact experiments was negligible compared to the structure's deformation (Lambert et al. 2009). Particles associated with the mesh were located at the intersections of wires, while particles associated with linear elements (i.e., cables and bars) were distributed along these elements

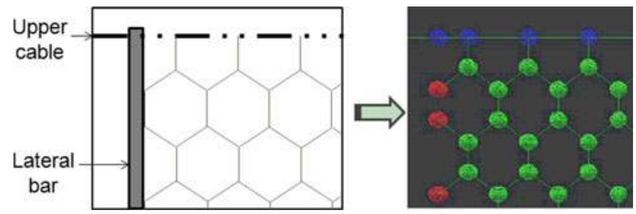

Fig. 5 Depending on their position in the structure, particles used in the DEM method are given different characteristics

(Fig. 5). The mass given to each particle depended on the type of element with which it was associated.

In this structure, five different interparticular link types can be distinguished: single wire of the wire mesh, double-twist wire of the wire mesh, bar, supporting cable, and cable connecting the trees and the bars. The forces associated with single and double-twist wires were computed using a specific interaction model available in Yade-DEM. The algorithm is based on the model proposed by Bertrand et al. (2008). It has been recently implemented into the software and has proved efficient in modelling the response of a hexagonal wire mesh in different conditions (Thoeni et al. 2013). The single wire stress-strain response considered in the model is identical to that given in Bertrand et al. (2008). As proposed by these authors, the stress-strain response curve of the double-twist wire is derived from that of the single wire one using the parameters λ_k and λ_ϵ. In this study, these parameters were given the value of 0.62 and 0.1, respectively.

Forces between particles located along the upper and lower cables were calculated considering an elastic model fully characterized by the cable diameter and its Young modulus (140 GPa). An elastoplastic model was considered for particles representing the cable between the tree and the bar to account for the sliding of the cable clips that was observed during the experiments. In the experiments, the cable tension was measured during block impacts using a dynamic force sensor installed in the top cable of the structure. The maximum cable tension measured, corresponding to sliding occurrence, was 40 kN (Lambert et al. 2009). The elastic model was, thus, considered for the cable until a threshold force $F_{\text{slip}} = 40$ kN was reached. Once this threshold value is reached, the interaction force remains equal to F_{slip} if the distance between particles increases. If the distance between particles decreases, the interaction force decreases following a linear strain–stress relationship with a Young modulus set at 140 GPa. The two bars at the extremities of the wire mesh were modelled as perfectly rigid assemblies of particles considering that the strains of these steel bars were negligible.

The impact by the block was modelled by considering a spherical element with a given mass and initial velocity. The interaction between the block and the mesh particles was modelled by contact forces considering an elastic normal contact law, with a block Young modulus of 100 GPa, and ignoring the block–fence friction. The resultant force on each particle of the mesh is, therefore, the sum of the contact forces with the projectile and of the interaction forces with the adjoining mesh particles. The force applied to the projectile is the sum of all contact forces with the wire mesh particles. In the first phase, a simulation under gravity loading is performed to reach the static equilibrium of the structure. Second, the impact is simulated. The spherical projectile is located at the impact point and initial kinematic conditions are applied to the projectile. For each impact simulation, the time evolution of the forces in the cables and on the projectile was recorded as well as the projectile trajectory.

The numerical model could be used to investigate the influence of parameters related to the block (mass, velocity, impact point, and inclination). The influence of various structural choices might also be investigated in an optimization process (single mesh dimensions, fence length, cable diameter). However, the direct use of this model for such exhaustive analyses cannot be envisaged in practice due to the long duration of each impact simulation. The approach proposed in the following is an alternative to using such models for this purpose.

3 Reliability-Based Fence Design

The fence design first consists in evaluating its efficiency in intercepting the block trajectory. This functional design aims at defining the height of the structure, mainly based on the block passing height determined based on trajectory simulations. Then the structural design is conducted, with the aim of assessing whether or not the structure efficiently stops the block once its trajectory is intercepted. The approach proposed for this purpose consists in estimating the probability of the block going over the fence given the distribution of the block's kinematics and properties (mass, most particularly). For that purpose a criterion for defining whether the block passes over the fence is first defined. Second, reliability analyses are done to calculate the probability of this limit criterion being reached.

3.1 Response Modes and Efficiency Criterion

Five different responses in terms of the post-impact block trajectory can potentially be observed in the simulations or the experiments:

- the block passes through the net (mode A),
- the block is sent uphill by the fence (mode B),
- the block is trapped in the fence, the wire mesh fringed by the lower cable forming a pocket containing the block (mode C),
- in an initial downward displacement relative to the fence, the block rotates while in contact with the fence and then goes under the lower cable (mode D),
- in an initial upward displacement relative to the fence, the block rotates while in contact with the fence before finally going over the upper cable (mode E).

Basically, in modes A, D and E, the block is not stopped, while in modes B and C, the block is stopped. Only mode A necessarily involves damage to the structure. The occurrence of one of these modes depends on the block's translational and rotational incident velocities, incident angle and impact point on the structure. Some modes are rare compared to others and require a very particular block kinematics (modes D and E). Mode E, which requires an impact close to the upper supporting cable by a block with an upward trajectory and high rotational velocity, was only observed in simulations with a spherical block if the upper cable was directly impacted. This was not observed during the experiments. On the contrary, mode D, requiring an impact close to the lower cable by a block with a downward trajectory, was observed in both simulations and experiments. However, the block velocity after going under the fence is small, resulting in the block generally stopping just after going under the fence. In addition, this situation can easily be avoided in practice, adding a wire mesh panel placed on the slope uphill of the fence, connected to its lower cable. The case where the block goes through the fence (mode A) is the most critical because the post-impact block trajectory is valley-side oriented with a possible high velocity.

The evolution of the block velocity during its interaction with the net fence can be considered to evaluate the fence efficiency. More precisely, the evolution of the sign of the horizontal component of the velocity during impact is a simple and straightforward way to assess the response of the fence in all the cases noted above. Indeed, if the block is trapped or pushed uphill by the fence, the horizontal velocity of the block is initially positive and decreases during impact to reach a nil or negative value after impact. On the contrary, if the block passes through, above or below the fence during impact, the horizontal velocity of the block decreases but does not reach negative or nil values.

This analysis naturally leads to considering $G = V_{z,\ \mathrm{out}}/V_{z,\ \mathrm{in}}$ as an estimator of the efficiency of the structure, where $V_{z,\ \mathrm{in}}$ and and $V_{z,\ \mathrm{out}}$ are the components along the horizontal z-axis of the block velocity before and after contact with the fence, respectively. $G \leq 0$ means that the block is stopped (safety domain, modes B and C). On the contrary, the block is not stopped if $G > 0$, according to modes A, D or E (failure domain).

4 Principles of the Reliability-Based Approach

This section presents the methodology used to characterize the probability $P_f = \text{Prob}(G > 0)$ for the fence failure using the DEM model of the fence. Contrary to classical Monte Carlo simulations, the approach proposed does not require covering all the parameter ranges. On the contrary, it allows calculating P_f using only a very small number of impact simulations, which ensures its practical feasibility.

The variability of the impact conditions can be characterized by a set of uncertain parameters y_i associated with the properties of the block (mass, shape) and its trajectory (impact velocities, impact point location). These parameters can be considered as the different components of a vectorial random variable $\mathbf{Y}$ with a probability density function p_y.

In this context, the mechanical response of the fence is modelled by a random variable $\mathbf{Z} = f(\mathbf{Y})$ to be characterized. In this study, this response is the estimator of the fence's efficiency $G = V_{z,\ \text{out}}/V_{z,\ \text{in}}$, called the "performance function". Assuming that $\mathbf{Y}$ can be related to a standard random variable $\mathbf{X}$ (Gaussian), such as $\mathbf{Y} = T(\mathbf{X})$, the performance function is expressed as $G = f \circ T(\mathbf{X})$. Appendix 2 provides an example of Gaussian standardization of two correlated log-normal random variables (Baroth et al. 2006).

If there is one uncertain input parameter $(Y_1) = \mathbf{Y}$, the performance function G may be approximated by writing the approximation $\tilde{G}$ of G as an expansion in Lagrange polynomials of a standard Gaussian random variable X_1 (Baroth et al. 2007), such that:

$$G(\mathbf{X}) \simeq \tilde{G}(X_1) = \sum_{i=1}^{N} G_i L_i(X_1), \tag{1}$$

where $G_i = G(x_i)$ is a set of N values of G and L_i are Lagrangian polynomials. $L_i(X_1)$ is written

$$L_i(X_1) = \prod_{\substack{k=1 \\ k \neq i}}^{N} \frac{X_1 - x_k}{x_i - x_k}. \tag{2}$$

Similarly, if there are two uncertain input parameters $(Y_1, Y_2) = \mathbf{Y}$, the performance function G may be approximated, such that:

$$G(\mathbf{X}) \simeq \tilde{G}(X_1, X_2) = \sum_{i=1}^{N} \sum_{j=1}^{N} G_{i,j} L_i(X_1) L_j(X_2), \tag{3}$$

where $G_{i,\ j} = G(x_i,\ x_j)$ is a set of N^2 values of G and L_i, L_j are Lagrangian polynomials.

The performance function can be calculated for a larger number of uncertain input parameters, although it will not be presented in the following.

The calculation of $P(G > 0)$ first requires defining the points x_i and x_j. $\mathbf{X}$ being a Gaussian standard random variable, we use roots of Nth-degree Hermite polynomials as the values of x_i and x_j (Press et al. 1994), given that they are orthogonal with respect to the Gaussian standard measure. The values of x_i for different values of N are given in Appendix 1.

Second, the values of $(y_i, y_j) = \mathbf{y}$ corresponding to the values of the $(x_i, x_j) = \mathbf{x}$ are determined using the relationships $\mathbf{y} = T(\mathbf{x})$. The values y_i and y_j depend on the statistical law associated with the random variable $\mathbf{Y}$ and on the number N of the points considered (Baroth et al. 2007). Appendix 2 details T with two correlated lognormal random variables.

Then, the values of the performance function $G(x_i)$ (resp. $G(x_i,\ x_j)$) are obtained from numerical simulations of impact on the fence using the set of parameters y_i (resp. $(y_i,\ y_j)$) corresponding to x_i (resp. $(x_i,\ x_j)$).

Finally, the numerical (and time-consuming) performance function G is approximated by the analytical function $\tilde{G}$. From this function, the cumulative distribution function and the probability $\text{Prob}(G > 0)$ can be evaluated.

4.1 Application to the Study Case

The impact conditions are characterized by the kinematical parameters of the block V_r, α_r, and ω_r and by the vertical and horizontal location of the impact point. Given the large number of random variables mentioned above and the potentially significant correlations between these variables, considering all the loading parameters as random variables can substantially increase the complexity of the assessment of the fence failure probability. In practice, the number of random variables considered has to be reduced. The choice of the parameters to be considered as random variables is crucial. This choice should account for the influence of the different parameters on the impact process and for the capacity of the rockfall model to accurately quantify these parameters.

Due to the resolution of the digital terrain model (4 m^2), the horizontal and vertical location of the impact point for the different block release simulations cannot be extracted precisely from the simulations. Both the horizontal and vertical location of the impact point are strongly related to micro-topographical changes that are not included in the digital terrain model due to its resolution. Given the potential errors on the estimation of the location of the impact point, it was assumed to be located in the centre of the fence. In addition, the rotational velocity ω_r was set at

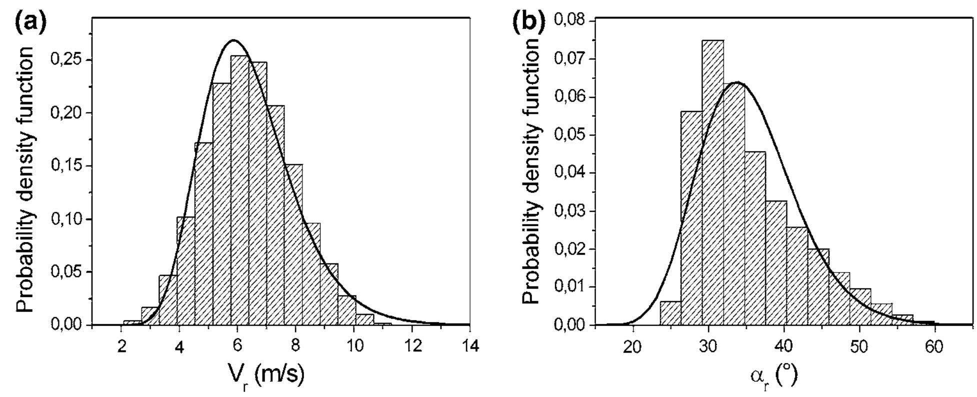

Fig. 6 Approximation of the simulated distributions of V_r and α_r by log-normal laws

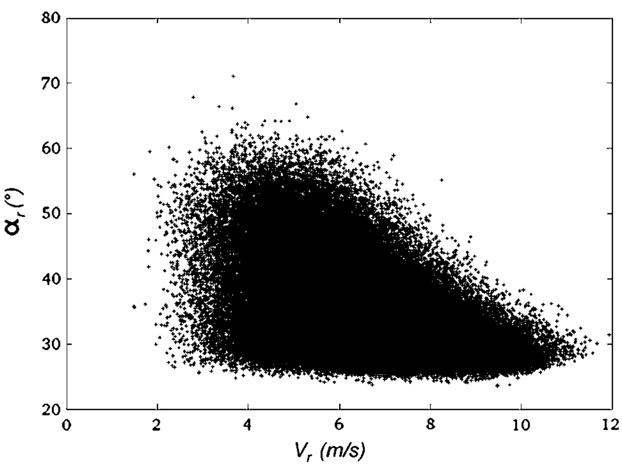

Fig. 7 Couples (V_r, α_r) obtained from rockfall simulations

Table 1 Means and coefficients of variation of the log-normal random variables associated with the velocity V_r and impact angle α_r, with correlation coefficient $\rho_{Y_1 Y_2} = -0.477$

Uncertain parameter	$Y_1 = V_r$	$Y_2 = \alpha_r$
Mean	$\mu_{Y\_1} = 6.42$ m/s	$\mu_{Y\_2} = 35.39°$
Coefficient of variation	$Cv_{Y\_1} = 0.25$	$Cv_{Y\_2} = 0.18$

the mean value obtained from rockfall simulations considering that this parameter had a second-order influence in the simulation results. This is justified by the low friction angle between the block and the fence and by the spherical shape of the block, resulting in a negligible influence of the rotational velocity on the block post-impact trajectory and on the fence's mechanical response. However, for different conditions, i.e., angular blocks and greater friction, the influence of the rotational velocity can become non-negligible (Tran et al. 2013). Finally, two variables are used for the impact simulations: the impact velocity V_r and the impact angle α_r.

As shown in Fig. 6, the probability density functions resulting from the trajectory analysis for these two parameters can be satisfactorily modelled using log-normal laws. Using the log-normal law is a satisfactory compromise taking into account the trend of histograms and preventing negative realizations (negative impact velocities, in particular) while allowing an easy probabilistic treatment.

Moreover, the different values of the couples (V_r, α_r) show a significant negative correlation between the two random variables (Fig. 7). For increasing values of V_r, decreasing mean values and variability of α_r are observed. This correlation can either be ignored or accounted for in evaluating fence efficiency. In the latter case, the correlation was modelled by considering a linear correlation with a coefficient of -0.477 between the two random variables. This coefficient was estimated from a principal component analysis of rockfall simulations, with a confident indicator (95 % confidence interval: $[-0.481, -0.472]$). This modelling remains a simple approximation of the complex correlations between the two variables, but it accounts for the general trends observed, i.e., decreasing mean values and variability of α_r for increasing values of V_r, from simple relationships. This simple model was used to evaluate the interest of accounting for the correlation. Table 1 presents the mean and coefficient of variation of the random variables considered and the correlation coefficient between them.

In the following, the influence of these two parameters on the efficiency of the fence will be studied first separately and then jointly. In the latter case, these two parameters are first considered as non-correlated before accounting for the linear correlation. For this reason, the two variables (namely the impact velocity $V_r = Y_1$ and the impact angle $\alpha_r = Y_2$) are modelled as two correlated log-normal random variables, denoted $(Y_1, Y_2) = \mathbf{Y}$. As detailed in Appendix 2, the Gaussian standardization of $\mathbf{Y}$, using the relation $\mathbf{Y} = T(\mathbf{X})$, is used to apply the collocation method. One or two non-correlated variables can be considered using this framework by using only the expression of Y_1 or setting the correlation coefficient $\rho_{Y_1 Y_2}$ at nil value, respectively.

Table 2 Sets of loading conditions used. Sets 1 to 5 correspond to loading conditions where only 1 random variable (r.v.) is considered

Set number	Number of simulations	Type	V_r	α_r	ω_r	Impact point	Block mass
1	5	1 r.v.	Lognormal distribution	20.72°	12.24 rad/s	Centred	476 kg
2	5			27.22°			
3	5			34.81°			
4	5			44.53°			
5	5			58.49°			
6	25	2 r.v.	Lognormal distribution	Lognormal distribution			
7	25	2 r.v.	Correlated lognormal distribution				

Sets 6 and 7 are associated with loading conditions considering 2 r.v., either non-correlated or correlated

Table 3 Values of the impact velocity $V_{r,i} = Y_{1,i}$ and the impact angle $\alpha_{r,\,j} = Y_{2,j}$ used in the simulation sets 1–6

$V_{r,\,i}$ (*m/s*)	3.10	4.47	6.23	8.69	12.55
$\alpha_{r,\,j}$ (°)	20.72	27.22	34.81	44.53	58.49

Table 4 Results of selected rockfall simulations for five different values of the velocity V_r and for an impact angle set at $\alpha_r = 34.8°$

$V_{r,i}$ (*m/s*)	3.10	4.47	6.23	8.69	12.55
$G\ (V_{r,i})$	–0.495	–0.516	–0.438	–0.258	0.529

The different sets of loading conditions used in the following are summarized in Table 2.

A 5-point procedure ($N = 5$, section 3.2) was used to analyse fence failure probability. This means that considering only one random variable, five impact simulations are required to estimate the failure probability. If two random variables are considered, a 5-point procedure requires performing impact simulations for all possible pairs of random variables using five different values of both random variables, corresponding to 25 impact simulations. For the sake of clarity, the choice of collocation points is illustrated for the case of one uncertain parameter in Appendix 1.

The simulations corresponding to the different sets of loading conditions were defined according to the principle defined in Table 2 and considering the values presented in Table 3 for the impact velocity and the impact angle. The results were analysed considering first the impact velocity V_r as the only random variable. The fence failure was analysed under this assumption for the different values of the impact angle α_r (Table 2, Simulation sets 1–5).

Second, the fence efficiency was analysed considering both parameters as non-correlated random variables (Table 2, Simulation set 6) and correlated random variables (Table 2, Simulation set 7). The impact velocity and impact angle corresponding to simulation sets 6 and 7 are compared in Fig. 8.

5 Probabilistic Analysis of Fence Efficiency

5.1 Influence of Velocity

Impact simulations for the five different values of the velocity V_r presented in Table 3 and for an impact angle set at $\alpha_r = 34.8°$ (simulation set 3, Table 2), corresponding to the mean impact angle in the rockfall simulations, are first analysed. The values of the performance function G obtained for these simulations are presented in

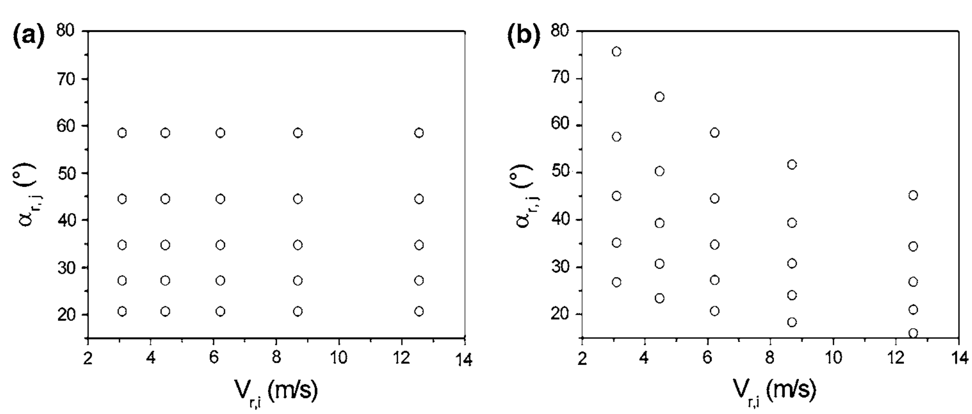

Fig. 8 Couples ($V_{r,i}$, $\alpha_{r,j}$) used for the generation of the simulation sets 6 and 7 composed of 25 impact simulations considering non-correlated (**a**) or correlated (**b**) random variables. Each *circle* corresponds to a specific couple ($V_{r,i}$, $\alpha_{r,j}$) used for one impact simulation

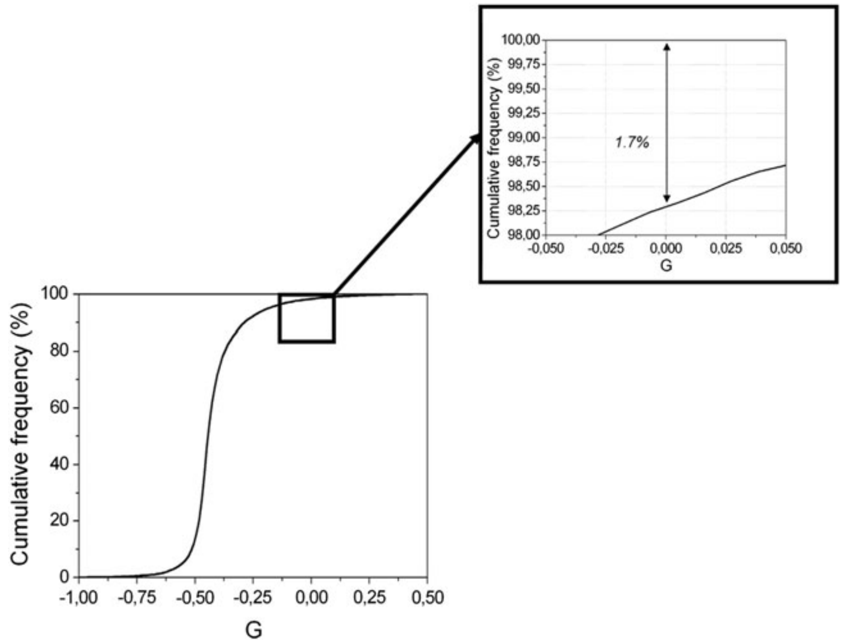

Fig. 9 Cumulative distribution of the performance function $G = \frac{V_{z,\mathrm{out}}}{V_{z,\mathrm{in}}}$ under loading conditions for which V_r is the only random variable

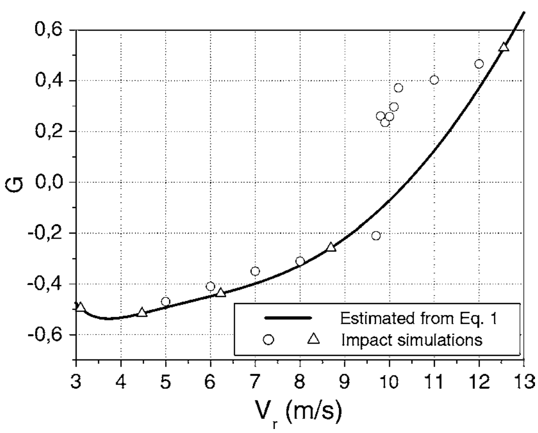

Fig. 10 Relationship between G and V_r either estimated from Eq. 1 or directly obtained from impact simulations. The values $G(V_{r,i})$ used for the estimation of $G(V_r)$ from Eq. 1 are associated with *triangular* symbols

Table 4. The fence does not fulfill its protection function and the block is not stopped when the velocity is 12.55 m/s ($G > 0$). The cumulative distribution of the performance function G considering only V_r as a random variable is given in Fig. 9. It clearly shows that the probability for having $G > 0$ is 1.7 %.

In addition, the relationship between G and V_r (Fig. 10) is characterized by interpolating the values $G(V_{r,i})$ (Table 4) using Eq. 1. The maximum velocity leading to fence efficiency, i.e., the velocity associated with $G(V_r) = 0$, is estimated from this relationship. This value is approximately $V_{r,\max}^{\mathrm{est.}} \approx 10.4$ m/s (Fig. 10) and corresponds to a maximum translational impact energy $E_{c,\max}^{\mathrm{est.}} = 1/2 m_{\mathrm{rock}} \, (V_{r,\max}^{\mathrm{est.}})^2 \approx 26$ kJ.

Additional impact simulations are done to assess the relevance of the approach, and in particular of the estimation of the maximum velocity leading to fence efficiency. These simulations allow directly characterizing the relationship between G and V_r. For these additional simulations, the loading conditions were the same as for the simulation set 3, except that the impact velocity V_r was set at different values ranging from 5 to 12 *m/s*. Although it is out of the scope of this paper to discuss in detail the mechanical response of the structure, one can note that the relationship between G and V_r characterized from impact simulations exhibits a strong non-linearity in the vicinity of $G(V_r) = 0$. In addition, the relationship obtained from these simulations exhibits significant differences with the relationship obtained from Eq. 1 in the vicinity of $G(V_r) = 0$ (Fig. 10). The maximum velocity leading to fence efficiency directly estimated from the impact simulations is approximately $V_{r,\max}^{\mathrm{dir.}} \approx 9.7$ m/s which corresponds to a maximum translational impact energy of $E_{c,\max}^{\mathrm{dir.}} = 1/2 m_{\mathrm{rock}} \, (V_{r,\max}^{\mathrm{dir.}})^2 \approx 23$ kJ. The difference between the method proposed and a direct assessment of the fence efficiency from impact simulations is approximately 7 % (resp. 13 %) in terms of maximum admissible impact velocity (resp. translational energy). The method proposed seems thus to be a compromise between the accuracy of the fence efficiency estimation and the computational effort, especially if a larger number of loading random variables has to be accounted for.

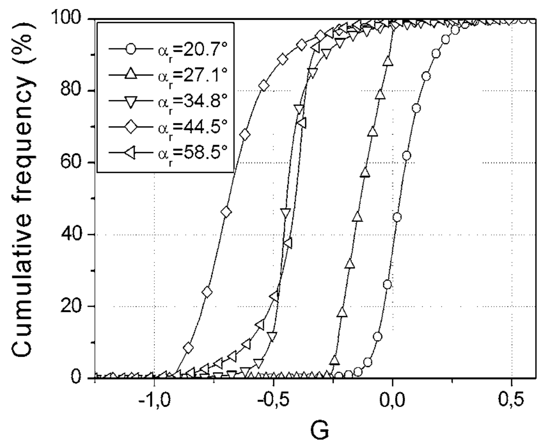

Fig. 11 Cumulative distribution function of the performance function G under loading conditions for which V_r is the only random variable and for different impact angles α_r

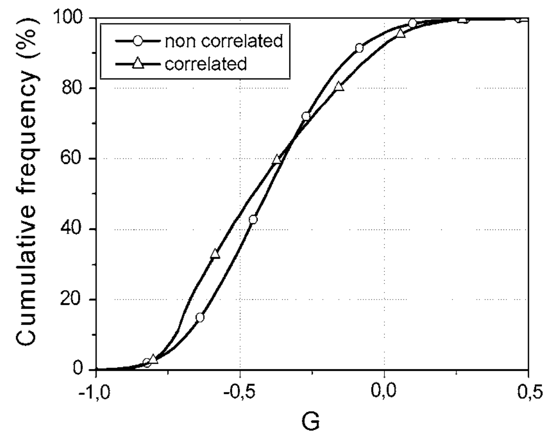

Fig. 12 Cumulative distribution function of the performance function G under loading conditions for which V_r and α_r are the only random variables

Table 5 Estimated maximum energy $E_{c,\max}^{\text{est.}}$ for different impact angles α_r

α_r (°)	20.7	27.1	34.8	44.5	58.5
$E_{c,\max}^{\text{est.}}$ (kJ)	7	18	26	27	30

5.2 Influence of the Two Variables, Considered as Non-Correlated

The results from the simulation sets 1 to 5 (Table 2) were analyzed considering the impact velocity as a random variable and the impact angle as a deterministic parameter, but for different impact angles. This analysis determined the cumulative distribution of the performance function G for different impact angles. This cumulative distribution function is strongly influenced by the impact angle (Fig. 11). The most critical cases, leading to larger probabilities for positive values of G, result from impacts oriented downwards and with shallow incidence with respect to the wire mesh plane.

For each value of the impact angle considered, the relationship between G and V_r is estimated from Eq. 1. The maximum admissible impact velocity and the corresponding translational impact energy were deduced following the same principle as illustrated above for an impact angle set at $\alpha_r = 34.8°$ (Figs. 9, 10). The estimated maximum admissible impact energy is shown to significantly depend on the impact angle considered (Table 5). In particular, the maximum admissible energy drastically decreases for shallow impacts.

Indeed, for the failure mode A, the net is loaded until tensile stresses develop along the surface of the wire mesh. Breakage occurs when these tensile stresses in the wire mesh are larger than the maximum admissible tensile stress of the mesh. The maximum admissible tensile stress is reached for larger block penetration into the net for normal impacts than for inclined ones, considering a centred impact point in both cases. Indeed, for normal impacts, the mesh surface able to strain before tensile stresses develop along the mesh surface is the same in the upper and lower parts of the net relative to the block location. For inclined impacts, the mesh surface able to strain before tensile stresses develop along the mesh surface is smaller either in the upper or in the lower part of the net relative to the block. Consequently, tensile stresses develop for smaller block penetrations for inclined impacts than for normal ones. As a result, the maximum admissible tensile stress of the mesh is reached for smaller block penetrations, corresponding to smaller boulder kinetic energy decreases, for inclined impacts.

5.3 Influence of the Two Variables, Considering the Correlation

The simulation set 7 (Table 2) characterized the cumulative distribution function of G considering the linear correlation between the two variables.

The fence failure probability in this case is calculated from the cumulative distribution functions of G (Fig. 12). The comparison with the case where the variables are considered non-correlated (simulation set 6, Table 2), plotted in the same figure, shows that not considering the correlation results in a smaller fence failure probability ($P(G > 0) = 4.2$ % without correlation and $P(G > 0) = 7.6$ % with correlation). Not considering the correlation between the two variables thus lead to optimistic results concerning the fence efficiency. The comparison with Fig. 9 shows that considering the only velocity as a random variable also leads to optimistic results with a fence failure probability of 1.7 % only.

6 Conclusion

In this paper, an approach aimed at improving the design of rockfall protection fences has been proposed. The design aspect concerned here is the ability of the fence to stop the block, provided the fence height has been appropriately determined. Traditionally, these structures are designed considering the energy of the block to be intercepted disregarding other parameters associated with block kinematics, mainly because it demands long computation times. On the contrary, the approach proposed herein aims at reducing the number of simulations to be performed while providing statistically relevant data with respect to fence efficiency, thus making more exhaustive studies affordable.

This approach combines block propagation simulations with numerical simulations of the fence impacted by the block. The use of trajectory simulation results ensures that the site-specific loadings are considered for the design of the fence. In addition, since the loading parameters are considered random variables, the variability of the loading conditions on the site is also introduced in the calculation for the fence design.

The feasibility of the approach was tested on a specific study case. The probability of a block going over a protection fence was examined considering variable loading of the fence related to two random variables: the impact velocity and the impact angle of the block. The fence failure probability was assessed considering successively one random variable (velocity), then the two variables considered non-correlated or linearly correlated.

The results obtained for the case study first show that the approach can be applied to calculate the probability of fence failure. The advantage for the designer also appears clearly. Classically, conducting a statistically relevant analysis considering two variables would require several hundred impact simulations, while only 25 are necessary with this approach.

The relevance of the method proposed has been evaluated in the case of one random variable. The method proposed constitutes a compromise in terms of computational effort and accuracy compared to the design of the fence directly from impact simulations. However, additional research work has to be done to assess more in detail the accuracy of the method, in particular for a larger number of loading random variables.

Conclusions concerning the response of the fence and its sensitivity to the variable considered can also be drawn. With only one random variable, a maximum allowable impact energy was estimated from the fence failure probability. However, this maximum impact energy strongly depends on the values of the deterministic loading parameters (most particularly, incidence angle). This quantity is, therefore, not an absolute indicator of fence capacity that can be generalized to different loading conditions, i.e., on another site.

The number of random variables strongly influences the probability of fence failure. If one random variable is considered, the probability of fence failure strongly depends on the values of the deterministic loading parameters. The impact angle has been shown to have a significant influence on fence failure probability, with a ratio of more than two over the impact angle range considered. This parameter should be considered when designing fences, together with the block mass and velocity.

This approach appears promising in terms of fence design improvement because it allows investigating the influence of many variables. It also improves the quantification of the residual hazard on the site after installing the structure. Neverthless, the influence of other parameters should be investigated, as for instance the impact point location on the fence, the block shape, and the orientation of the block with respect to the fence's perpendicular axis.

Acknowledgments This research was conducted within the framework of the Natural Hazards and Vulnerability of Structures (VOR) research network. This network is funded by the French Ministry of Research and joins different laboratories in the Rhônes-Alpes region.

Appendix 1: Roots of Hermite Polynomials

The values of x_i, corresponding to the roots of Nth-degree Hermite polynomials, denoted H_N, should be computed numerically or found in tables (Press et al. 1994). For instance, Table 6 provides points x_i for $N = 3$, 4, 5, where $H_3(x) = x^3 - 3x$, $H_4(x) = x^4 - 6x^2 + 3$, $H_5(x) = x^5 - 10x^2 + 15x$. Such values are classically deduced from quadrature formulas (see also Baroth et al. 2007).

Table 6 Points x_i for $N = 3$, 4, 5

Points	$N = 3$	$N = 4$	$N = 5$
x_1	$-\frac{\sqrt{6}}{2}$	$-\sqrt{\frac{3+\sqrt{6}}{2}}$	−2.0202
x_2	0	$-\sqrt{\frac{3-\sqrt{6}}{2}}$	−0.9586
x_3	$\frac{\sqrt{6}}{2}$	$\sqrt{\frac{3-\sqrt{6}}{2}}$	0
x_4	–	$\sqrt{\frac{3+\sqrt{6}}{2}}$	0.9586
x_5	–	–	2.0202

Appendix 2: Gaussian Standardization of Two Correlated Log-Normal Random Variables

Let $\mathbf{Y} = (Y_1, Y_2)$ be a 2D lognormal random variable with given mean $\mu_Y = (\mu_{Y\_1}, \mu_{Y\_2})$ and standard deviation $\sigma_Y = (\sigma_{Y\_1}, \sigma_{Y\_2})$ and coefficient of correlation $\rho_{Y\_1\ Y\_2}$. In this case, the Gaussian standardization of $\mathbf{Y}$ is written (Baroth et al. 2006):

$$\mathbf{Y} = T(\mathbf{X}) \Leftrightarrow \begin{cases} Y_1 = \frac{\mu_{Y_1}}{\sqrt{1+\mathrm{Cv}_{Y_1}^2}} \exp\{L_{11}X_1\} \\ Y_2 = \frac{\mu_{Y_2}}{\sqrt{1+\mathrm{Cv}_{Y_2}^2}} \exp\{L_{21}X_1 + L_{22}X_2\} \end{cases}, \tag{4}$$

with:

$$L_{11} = \sqrt{\ln(1 + \mathrm{Cv}_{Y_1}^2)}, \tag{5}$$

$$L_{21} = \frac{\ln(1 + \rho_{Y_1Y_2}\mathrm{Cv}_{Y_1}\mathrm{Cv}_{Y_2})}{L_{11}}, \tag{6}$$

$$L_{22} = \sqrt{\frac{\ln(1 + \mathrm{Cv}_{Y_1}^2)\ln(1 + \mathrm{Cv}_{Y_2}^2) - \ln^2(1 + \rho_{Y_1Y_2}\mathrm{Cv}_{Y_1}\mathrm{Cv}_{Y_2})}{L_{11}^2}}, \tag{7}$$

where $\mathrm{Cv}_{Y_i} = \frac{\sigma_{Y_i}}{\mu_{Y_i}}, i = 1, 2$ are the coefficients of variation of Y_1 and Y_2.

References

Agliardi F, Crosta GB, Frattini P (2009) Integrating rockfall risk assessment and countermeasure design by 3D modelling techniques. Nat Hazards Earth Syst Sci 9:1059–1073

Baroth J, Schoefs F, Breysse D (2012) Construction reliability. Wiley, London

Baroth J, Bressolette P, Chauviere C, Fogli M (2007) An efficient SFE method using Lagrange polynomials: application to nonlinear mechanical problems with uncertain parameters. Comp Meth Appl Mech Eng 196:4419–4429

Baroth J, Bode L, Bressolette P, Fogli M (2006) SFE method using Hermite polynomials: an approach for solving nonlinear mechanical problems with uncertain parameters. Comp Meth Appl Mech Eng 195(44–47):6479–6501

Bertrand D, Nicot F, Gotteland P, Lambert S (2008) DEM numerical modeling of double-twisted hexagonal wire mesh. Can Geotech J 45:1104–1117

Bertrand D, Trad A, Limam A, Silvani C (2012) Full-scale dynamic analysis of an innovative rockfall fence under impact by the discrete element method. From the local scale to the structure scale. Rock Mech Rock Eng 45(5):885–900

Bourrier F, Dorren LKA, Nicot F, Berger F, Darve F (2009) Toward objective rockfall trajectory simulation using a stochastic impact model. Geomorphology 110:6879

Bourrier F, Bigot C, Bertrand D, Lambert S, Berger F (2010) A numerical model for the design of low energy rockfall protection nets. In: Proceedings of the third Euro-Mediterranean symposium on avances in geomaterials and structures, Djerba, Tunisia

Buzzi O, Spadari M, Giacomini A, Fityus S, Sloan SW (2012) Experimental testing of rockfall barriers designed for the low range of impact energy. Rock Mech Rock Eng. doi:10.1007/s00603-012-0295-1

Cazzani HG, Mongiovi L, Frenez T (2002) Dynamic finite element analysis of interceptive devices for falling rocks. Int J Rock Mech Min 39:303–321

Crosta GB, Agliardi F (2004) Parametric evaluation of 3D dispersion of rockfall trajectories. Nat Hazards Earth Syst Sci 4:583–598

Cundall PA, Strack ODL (1979) A discrete numerical model for granular assemblies. Geotechnique 29((1):47–65

Dorren LKA, Berger F, Putters US (2006) Real size experiments and 3D simulation of rockfall on forested and non-forested slopes. Nat Hazard Earth Sys 6:145–153

EOTA (2008) Guidelines for European technical approval of falling rock protection kits (ETAG 027), Brussels

Gerber W, Boell A (2006) Type-testing of rockfall barriers-comparative results. In: International proceedings of the interpraevent congress, Nigata, Japan

Gentilini C, Govoni L, Miranda S, Gottardi G, Ubertini F (2012) Three-dimensional numerical modelling of falling rock protection barriers. Comput Geotech 44:58–72

Gottardi G, Govoni L (2010) Full-scale modelling of falling rock protection barriers. Rock Mech Rock Eng 43(3):261–274

Grassl H, Volkwein A, Anderheggen E, Ammann WJ (2002) Steel-net rockfall protection—experimental and numerical simulations. In: Proceedings of the seventh international conference on structures under shock and impact, Montreal, Canada

Hearn G, Barrett RK, Henson HH (1996) Testing and modelling of two rockfall barriers. Transp Res record 1504:1–11

Lambert S, Bertrand D, Berger F, Bigot C (2009) Low energy rockfall protection fences in forested areas: experiments and numerical modeling. In: Prediction and simulation methods for geohazard mitigation, Kyoto, Japan

Lambert S, Bourrier F (2013) Design of rockfall protection embankments: a review. Eng Geol 154:77–88

Nicot F, Cambou B, Mazzoleni G (2001) Design of rockfall restraining nets from a discrete element modelling. Rock Mech Rock Eng 34:98–118

Peila D, Pelizza S, Sassudelli F (1998) Evaluation of behaviour of rockfall restraining nets by full scale tests. Rock Mech Rock Eng 21(1):1–24

Press WH, Teukolsky SA, Vetterling WT, Flannery BP (1994) Numerical recipes in Fortran, 2nd edn. Cambridge University Press, Cambridge

Sasiharan B, Muhunthan B, Badger TC, Shua S, Carradine DM (2006) Numerical analysis of the performance of wire mesh and cable net rockfall protection systems. Eng Geol 8(1–2):121–132

Smilauer V, Catalano E, Chareyre B, Dorofeenko S, Duriez J, Gladky A, Kozicki J, Modenese C, Scholtes L, Sibille L, Stransky J, Thoeni K (2010) Yade documentation. In: Smilauer V (ed) The Yade project, 1st edn. http://yade-dem.org/doc/

Spadari M, Kardani M, De Carteret R, Giacomini A, Buzzi O, Fityus S, Sloan SW (2013) Statistical evaluation of rockfall energy ranges for different geological settings of New South Wales, Australia. Eng Geol 158:57–65

Stokes A, Salin F, Kokutse AD, Berthier S, Jeannin H, Mochan S, Dorren LKA, Kokutse N, Abd-Ghani M, Fourcaud T (2005) Mechanical resistance of different tree species to rockfall in the French Alps. Plant Soil 278(1–2):107–117

Thoeni K, Lambert C, Giacomini A, Sloan SW (2013) Discrete modelling of hexagonal wire meshes with a stochastically distorted contact model. Comput Geotech 49:158–169

Tran VP, Maegawa K, Fukada S (2013) Experiments and dynamic finite element analysis of a wire-rope rockfall protective fence. Rock Mech Rock Eng 46:1183–1198

Volkwein A, Roth A, Gerber W, Vogel A (2009) Flexible rockfall barriers subjected to extreme loads. Struct Eng Int 19:327–332